Measuring and Modeling Anisotropic Reflection

Gregory J. Ward
Lighting Systems Research Group
Lawrence Berkeley Laboratory

ABSTRACT

A new device for measuring the spatial reflectance distributions of surfaces is introduced, along with a new mathematical model of anisotropic reflectance. The reflectance model presented is both simple and accurate, permitting efficient reflectance data reduction and reproduction. The validity of the model is substantiated with comparisons to complete measurements of surface reflectance functions gathered with the novel reflectometry device. This new device uses imaging technology to capture the entire hemisphere of reflected directions simultaneously, which greatly accelerates the reflectance data gathering process, making it possible to measure dozens of surfaces in the time that it used to take to do one. Example measurements and simulations are shown, and a table of fitted parameters for several surfaces is presented.

General Terms: algorithms, measurement, theory, verification. **CR Categories and Descriptors:** I.3.7 Three-dimensional graphics and realism, I.6.4 Model validation and analysis. **Additional Keywords and Phrases:** reflectance, Monte Carlo, raytracing, shading.

1. Introduction

Numerous empirical and theoretical models for the local reflection of light from surfaces have been introduced over the past 20 years. Empirical and theoretical models have the same goal of reproducing real reflectance functions, but the respective approaches are very different.

An empirical model is simply a formula with adjustable parameters designed to fit a certain class of reflectance functions. Little attention is paid to the physical derivation of the model, or the physical significance of its parameters. A good example of an empirical model is the one developed by Sandford [Sandford85]. This is a four parameter model of isotropic reflection, where the parameters must be fit to a specific set of reflectance measurements. While two of these parameters correspond roughly to measurable quantities such as total reflectance and specularity, the other two parameters have no physical significance and are merely shape variables that make the specular lobe of the model more closely match the data.

In contrast to an empirical model, a theoretical model attempts to get closer to the true distribution by starting from physical theory. A good example of a theoretical model is the one derived recently by He et al [He91]. This is also a four parameter isotropic model, but all four parameters have some physical meaning and can in principle be measured *separately from the surface reflectance distribution*. In practice, however, it is usually necessary to fit even a theoretical model to measurements of reflectance because the physical parameters involved are difficult to measure. This is the case in the He-Torrance model, since measurements of the requisite surface height variance and auto-

Author's address: 1 Cyclotron Rd., 90-3111, Berkeley, CA 94720.
E-mail: GJWard@lbl.gov

correlation distance variables are impractical for most surfaces. Thus, the physical derivation of such a model serves primarily to inspire greater confidence, and is not necessarily a practical advantage when it comes to fitting measured data. As in all scientific disciplines, if the theory does not fit the data, then the theory must be discarded, not the data.

But where is the data? There is almost no published data on surface reflectance as a function of angle, and what little data is available is in the form of plane measurements of isotropic surfaces with no rotational variance in their reflectance functions. Thus, we have little to compare our reflectance models to, and no real assurance that they are valid. This means that we may once again be falling back on the "if it looks reasonable then it's OK" philosophy that has misdirected computer graphics so often in the past.

Why is the oldest specular model, the one introduced by Phong in 1975 [Phong75], still the most widely used to this day? This model is neither theoretically plausible nor empirically correct. Any renderings that use the straight Phong model are most likely wrong because the model is not physical, and more light may be emitted than is received (for example). The sole virtue of the Phong model is its mathematical simplicity.

Simplicity is indispensable in computer graphics. Simplicity is what permits fast renderings and hardware implementations. Without it, a reflectance model is little more than a novelty. Even a relatively straightforward model such as the one developed by Torrance and Sparrow [Torrance67] and tailored for rendering applications by Blinn [Blinn77] and later Cook [Cook82] has been underutilized in computer graphics due to its moderately complex form. More recent introductions by Poulin and Fournier [Poulin90] as well as He et al [He91] are even more complex. What is really needed for computer graphics is a simple reflectance model that works reasonably well for most materials.

Our goal in this paper is not to present the ultimate mathematical model of reflectance, but to provide a simple formula that is physically valid and fits measured reflectance data. Here we will present both a new method for measuring isotropic and anisotropic reflectance distributions and a mathematical model that fits these data with both accuracy and simplicity.

2. Definition of the BRDF

The interaction of light with a surface can be expressed as a single function, called the *bidirectional reflectance distribution function*, or BRDF for short [Nicodemus77]. This is a function of four angles, two incident and two reflected, as well as the wavelength and polarization of the incident radiation. For the sake of simplicity, we will leave wavelength and polarization out of our equations, but keep in mind that they are contained implicitly in the function ρ_{bd}, which is defined in terms of incident and reflected radiance by the following integral:

$$L_r(\theta_r,\phi_r) = \int_0^{2\pi} \int_0^{\pi/2} L_i(\theta_i,\phi_i)\, \rho_{bd}(\theta_i,\phi_i;\theta_r,\phi_r)\, \cos\theta_i\, \sin\theta_i\, d\theta_i\, d\phi_i \qquad (1)$$

where: ϕ is the azimuthal angle measured about the surface normal

$L_r(\theta_r,\phi_r)$ is the reflected radiance (watts/steradian/meter^2)

$L_i(\theta_i,\phi_i)$ is the incident radiance

$\rho_{bd}(\theta_i,\phi_i;\theta_r,\phi_r)$ is the BRDF (steradian^{-1})

The function ρ_{bd} is *bidirectional* because the incident and reflected directions can be reversed and the function will return the same value. This arises from the fact that the physics of light is the same run backwards as forwards, which is why light-backwards ray tracing works [Whitted80].

3. Measuring the BRDF of a Surface

A device for measuring BRDFs is called a *gonioreflectometer*. The usual design for such a device incorporates a single photometer that is made to move in relation to a surface sample, which itself moves in relation to a light source, all under the control of a computer. Because BRDFs are in general a function of four angles, two incident and two reflected, such a device must have four degrees of mechanical freedom to measure the complete function. This requires substantial complexity in the apparatus and long periods of time to measure a single surface. A typical gonioreflectometer arrangement, designed by Murray-Coleman and Smith [Murray-Coleman90], is shown in Figure 1.
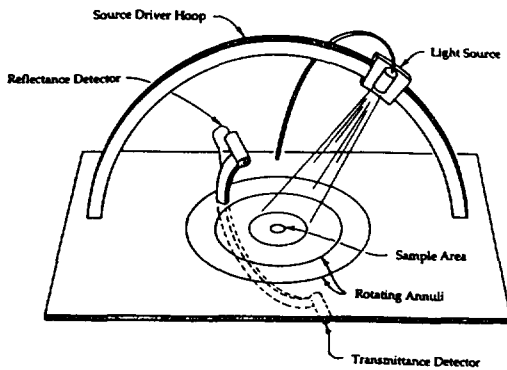

Figure 1. A conventional gonioreflectometer with movable light source and photometer.

As an alternative to building such a gonioreflectometer, there are several labs in North America where one can send a surface sample for BRDF characterization. For a few hundred dollars, one can get a three plane measurement of an isotropic material at four or five angles of incidence. (An isotropic material has a BRDF that is independent of rotation about the the normal. Therefore, only one ϕ_i direction is sampled.) Unfortunately, a comprehensive BRDF measurement of an anisotropic surface typically costs a few *thousand* dollars. (An anisotropic material reflects light differently at different angles of rotation, thus multiple ϕ_i directions must be sampled.) Because of the difficulty and expense of the BRDF measurements themselves, only the very richest research programs can afford their own data. This data is essential, however, for the correct modeling of surface reflectance.

3.1. An Imaging Gonioreflectometer

The Lighting Systems Research Group at Lawrence Berkeley Laboratory has developed a relatively simple device for measuring BRDFs that uses imaging technology to obtain results more quickly and at a lower cost than conventional methods. This *imaging gonioreflectometer* has been developed over the past three years and represents an important advance towards the more practical characterization of BRDFs for lighting simulation and computer graphics. It is our hope that other laboratories and research institutions will construct their own versions of this apparatus and thereby make BRDF measurement a more common and economical practice.

The basic arrangement of the LBL imaging gonioreflectometer is shown in Figure 2†. The key optical elements are a half-silvered hemisphere or hemi-ellipsoid and a charge-coupled device (CCD) camera with a fisheye lens. Combined, these elements take care of the two degrees of freedom handled by a mechanically controlled photometer in a conventional gonioreflectometer. Light reflected off the sample surface in
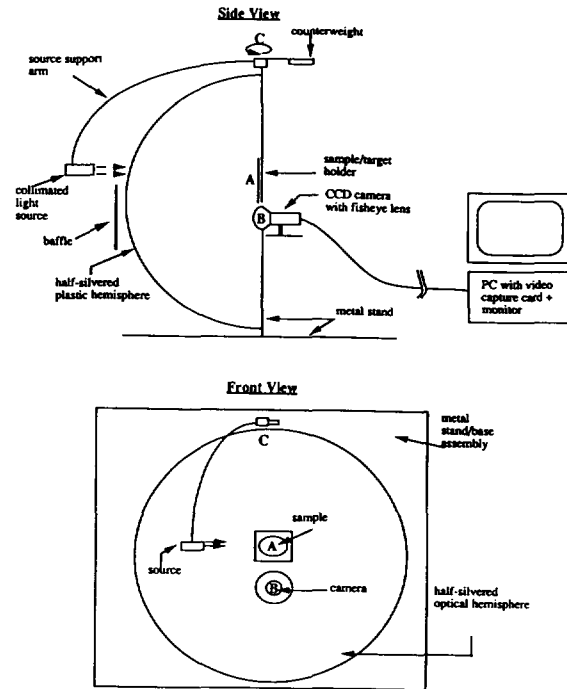

Figure 2. The LBL imaging gonioreflectometer.

holder A is collected by the hemispherical mirror and reflected back into the fisheye lens and onto the CCD array B. By focusing the lens at one half the hemisphere radius, a near perfect imaging of the reflected angles takes place. (See ray diagram in Figure 3.) Because of this highly efficient collector arrangement, the light source does not have to be very bright to obtain a good measurement, and can thus be optimized for collimation to get the best possible angular resolution. In our device, a 3-watt quartz-halogen lamp is used with an optically precise parabolic reflector to produce a well collimated beam. White light is preferable for photopic measurements, although an array of colored filters may be used to measure the spectral dependence of the BRDF. The hemisphere is half-silvered to allow the light beam to illuminate the sample, and an exterior baffle shields the camera from stray radiation. This unique arrangement of light source and optics allows retroreflection (light reflected back towards the light source) and transmission to be measured as well.

The incident θ_i and ϕ_i angles are controlled mechanically by pivoting the light source arm at point C and the sample holder at point A, respectively. In our current prototype, the light source is moved by a computer-controlled motor during data collection, and the sample is rotated manually. Because the hemisphere of reflected directions is captured in a single image, data collection proceeds quite rapidly and a complete BRDF can be recorded in a few minutes, including time for manual rotation of the sample.

3.2. Calibration and Data Reduction

All measurements are made relative to a standard diffuse sample and a background measurement. The background measurement is made with the source on but without any sample in the holder (using the dark room behind to simulate a black body), and is subtracted from the other measurements to reduce the effects of stray and ambient light. The standard sample measurement is used as a basis for obtaining absolute reflectance values using the following simple equation at each image point:

$$\rho_{bd} = \frac{v_{measured} - v_{background}}{v_{standard} - v_{background}} \cdot \frac{\rho_{standard}}{\pi} \qquad (2)$$

where:

$\rho_{standard}$ is the total diffuse reflectance of the standard sample

The ability to measure absolute BRDF values directly is an important feature of the imaging gonioreflectometer. Most other devices rely on auxiliary measurements of directional reflectance (ie. total reflectance for
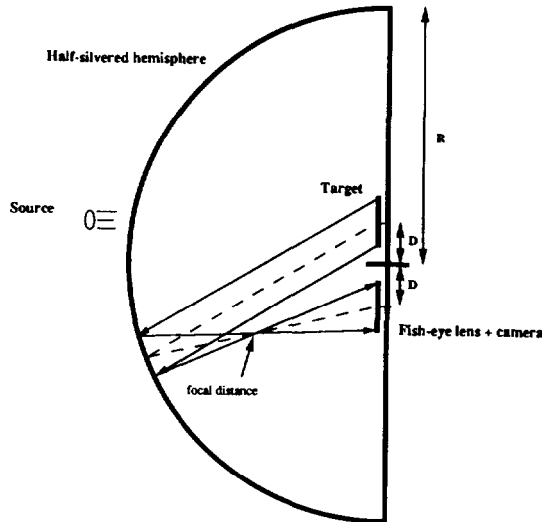
Figure 3. Imaging gonioreflectometer geometry. Light reflected by the sample in a specific direction is focused by the hemisphere or hemi-ellipsoid through a fisheye lens onto a CCD imaging array.

light incident at some (θ_i, ϕ_i)) and numerical integration to arrive at absolute quantities.

Recovering the reflected angles from pixel locations in the captured image is accomplished in two steps. The first step is to determine the mapping from image point locations to the lens incident direction. This is a function of the particular fisheye lens used, the camera, and the video capture board. Since this mapping varies so much from one implementation to the next and is easily measured, we will not discuss it any further here. The second step is to compute the target reflection angles from these camera incident angles. Figure 3 shows the geometry involved, and after a bit of trigonometry one can derive the following approximation:

$$r_c = D \sin\phi_c \sin\theta_c + \sqrt{D^2 \sin^2\phi_c \sin^2\theta_c + R^2 - D^2}$$

$$\theta_r = \cos^{-1}\left[\frac{r_c \cos\theta_c}{\sqrt{r_c^2\cos^2\phi_c \sin^2\theta_c + (r_c \sin\phi_c \sin\theta_c - 2D)^2 + r_c^2 \cos^2\theta_c}}\right] \quad (3)$$

$$\phi_r = \tan^{-1}\left[r_c \sin\phi_c \sin\theta_c - 2Dr_c \cos\phi_c \sin\theta_c\right]$$

where:

θ_r is polar angle relative to target

ϕ_r is azimuthal angle relative to target, right is 0°

θ_c is polar angle relative to camera

ϕ_c is azimuthal camera angle, right is 0°

R is radius of sphere or approximate radius of ellipsoid

D is one half the separation between target and camera centers

r_c is an intermediate result which is the distance from camera to reflector

notes:

The arctangent in the above equation should be computed using the signs of the numerator and denominator to get a range of 360°. Many math libraries provide a function named atan2 for this purpose.

The above equations are a good approximation both for hemispherical and hemi-ellipsoidal reflectors as long as D is small in relation to R.
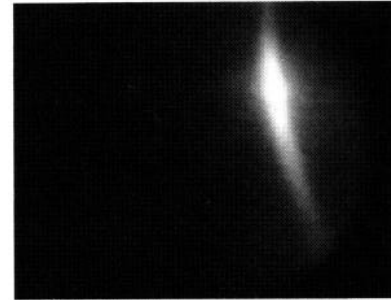

Figure 4. An image captured by the gonioreflectometer from an unfinished aluminum sample.

The image captured by our gonioreflectometer for a piece of unfinished aluminum illuminated at $(\theta_i, \phi_i) = (30°, 0°)$ is shown in Figure 4. Although the image was reduced before data reduction to a resolution of 108 by 80 pixels, there is still much more information than is needed for an accurate lighting simulation. Also, since two or more f-stops may be used to capture the full dynamic range of the BRDF, there is often redundant information where the useful ranges of exposures overlap. We therefore apply a program to eliminate crowding of data points and insure that the peak is recorded at a high enough angular resolution while the rest of the usable distribution is recorded at a uniform density. A data fitting program can then be used to match the reduced data set to a specific reflectance model.

3.3. Measurement Limitations

Our current implementation of the imaging gonioreflectometer has two main limitations in its measurement abilities. First, we are limited in our ability to measure the reflectance function near grazing angles, due to the size and shape of our reflecting hemisphere and the size of our sample. Our present hemisphere is formed from acrylic plastic and its optical properties are less than perfect, especially near the edges. It should be possible to partially overcome this limitation by placing the sample at right angles to its current configuration and illuminating it through the target holder, but this has not yet been tried. The ultimate solution would be to go to a larger, more precise hemisphere and a larger sample target.

The second limitation is our inability to measure more polished surfaces with sharp specular peaks. Again, the optical precision of our hemisphere is a problem, but so is the finite collimation of our light source. A highly uniform, collimated light source is required for the measurement of polished surfaces. That is why many commercial gonioreflectometers employ a laser, despite the laser's inability to yield spectrally balanced measurements. By using an incandescent source with an even smaller filament, it should be possible to measure more polished surfaces without resorting to a laser.

Note that the BRDF of a perfectly smooth surface is not directly measurable by any gonioreflectometer, since it is a Dirac delta function with an infinite value at a single point. Measuring such a BRDF of such a surface is not required however, since the physics of smooth surfaces are well understood and measurements of total reflectance are adequate for their characterization.

4. Modeling Anisotropic Reflectance

Armed with a device that can measure anisotropic reflectance functions economically, we need a mathematical model that can be fit to our newfound data. Using the data directly is impractical because it requires too much memory, and oftentimes the data is noisy and not complete enough to cover the entire domain of the BRDF. We could represent the BRDF as a sum of 100 or so terms in a spherical harmonic series, but this would also be expensive in terms of computation time and of memory [Cabral87][Sillion91]. We would prefer a model that fits the data with as few parameters as possible. Ideally, these parameters would be either physically derived or meaningful so that they could be set manually in the absence of any data at all.

Many models have been suggested for isotropic reflection, but only a few models have been published for the more general anisotropic case. Kajiya published a fairly robust method for deriving BRDFs of metals

from surface microstructure [Kajiya85]. However, his approach is not amenable to fitting measured reflectance data because the parameter space is too large (ie. all possible surface microstructures) and the BRDFs take too long to compute. Poulin and Fournier developed a model based on cylindrical scratches that is better suited [Poulin90], but their model is restricted to a specific microstructure with cross-sectional uniformity, and its evaluation is still somewhat expensive.

Our goal is to fit our measured reflectance data with the simplest empirical formula that will do the job. If we can develop a model with physically meaningful parameters without adding undue complexity, so much the better.

4.1. The Isotropic Gaussian Model

The Gaussian distribution has shown up repeatedly in theoretical formulations of reflectance [Beckmann63][Torrance67][Cook82], and it arises from certain minimal assumptions about the statistics of a surface height function. It is usually preceded by a Fresnel coefficient and geometrical attenuation factors, and often by an arbitrary constant. Since the geometric attenuation factors are typically difficult to integrate and tend to counteract the Fresnel factor anyway, we have replaced all of these coefficients with a single normalization factor that simply insures the distribution will integrate easily and predictably over the hemisphere.

$$\rho_{bd\_iso}(\theta_i,\phi_i;\theta_r,\phi_r) = \frac{\rho_d}{\pi} +$$
$$\rho_s \cdot \frac{1}{\sqrt{\cos\theta_i \cos\theta_r}} \cdot \frac{\exp[-\tan^2\delta/\alpha^2]}{4\pi\alpha^2} \quad (4)$$

where:

ρ_d is the diffuse reflectance

ρ_s is the specular reflectance

δ is the angle between vectors $\hat{n}$ and $\hat{h}$ shown in Figure 5

α is the standard deviation (RMS) of the surface slope

notes:

The ρ values may have some spectral dependence, and this dependence may vary as a function of angle so long as $\rho_d + \rho_s$ (the total reflectance) is less than 1. Thus, Fresnel effects may be modeled if desired.

The normalization factor, $\frac{1}{4\pi\alpha^2}$, is accurate as long as α is not much greater than 0.2, when the surface becomes mostly diffuse.

The main difference between this isotropic Gaussian reflectance model and that of Phong is its physical validity. For example, most Phong implementations do not have the necessary bidirectional characteristics to constitute a valid BRDF model. It is clear by inspection that the above formula is symmetric with respect to its incident and reflected angles. Without this symmetry, a BRDF model cannot possibly be physical because the simulated surface reflects light differently in one direction than the other, which is forbidden by natural law. Also, without proper normalization, a reflectance model does not yield correct energy balance and thus cannot produce physically meaningful results. Even

the model introduced recently by He et al [He91] with its rigorous physical derivation does not seem to pay close enough attention to normalization. Specifically, the so-called ambient term in the He-Torrance model is added without regard to the overall reflectance of the material, which by nature of the model is very difficult to compute. Comparisons were not made in He's paper between the reflectance model and absolute BRDF measurements (the data was scaled to match the function), thus normalization was not even demonstrated empirically. The fact that normalization was not adequately treated in He's otherwise impeccable derivation shows just how much normalization is overlooked and undervalued in reflectance modeling. The simplicity of the model presented here is what allows us to incorporate built-in normalization and has other desirable features as well, such as permitting quick evaluation for data reduction and Monte Carlo sampling.

4.2. The Anisotropic (Elliptical) Gaussian Model

It is relatively simple to extend the Gaussian reflectance model to surfaces with two perpendicular (uncorrelated) slope distributions, α_x and α_y. The normalized distribution is as follows:

$$\rho_{bd}(\theta_i,\phi_i;\theta_r,\phi_r) = \frac{\rho_d}{\pi} +$$
$$\rho_s \cdot \frac{1}{\sqrt{\cos\theta_i \cos\theta_r}} \cdot \frac{\exp[-\tan^2\delta(\cos^2\phi/\alpha_x^2 + \sin^2\phi/\alpha_y^2)]}{4\pi\alpha_x\alpha_y} \quad (5a)$$

where:

ρ_d is the diffuse reflectance

ρ_s is the specular reflectance

α_x is the standard deviation of the surface slope in the $\hat{x}$ direction

α_y is the standard deviation of the surface slope in the $\hat{y}$ direction

δ is the angle between the half vector, $\hat{h}$ and the surface normal, $\hat{n}$.

ϕ is the azimuth angle of the half vector projected into the surface plane.

A computationally convenient approximation for ρ_{bd} is:

$$\rho_{bd}(\theta_i,\phi_i;\theta_r,\phi_r) = \frac{\rho_d}{\pi} +$$
$$\rho_s \cdot \frac{1}{\sqrt{\cos\theta_i \cos\theta_r}} \cdot \frac{1}{4\pi\alpha_x\alpha_y} \exp\left[-2\frac{\left[\frac{\hat{h}\cdot\hat{x}}{\alpha_x}\right]^2 + \left[\frac{\hat{h}\cdot\hat{y}}{\alpha_y}\right]^2}{1 + \hat{h}\cdot\hat{n}}\right] \quad (5b)$$

where:

$$\hat{h}\cdot\hat{x} = \frac{\sin\theta_r\cos\phi_r + \sin\theta_i\cos\phi_i}{||\vec{h}||}$$

$$\hat{h}\cdot\hat{y} = \frac{\sin\theta_r\sin\phi_r + \sin\theta_i\sin\phi_i}{||\vec{h}||}$$

$$\hat{h}\cdot\hat{n} = \frac{\cos\theta_r + \cos\theta_i}{||\vec{h}||}$$

$$||\vec{h}|| = \left[2 + 2\sin\theta_r\sin\theta_i(\cos\phi_r\cos\phi_i + \sin\phi_r\sin\phi_i) + 2\cos\theta_r\cos\theta_i\right]^{\frac{1}{2}}$$

For vector calculations, the following substitutions are used:

$$\vec{h} = \hat{d}_r + \hat{d}_i$$

$$\hat{h} = \frac{\vec{h}}{||\vec{h}||}$$

$$\cos\theta_r = \hat{d}_r \cdot \hat{n}$$

$$\cos\theta_i = \hat{d}_i \cdot \hat{n}$$

where:

$\hat{d}_r$ is the reflected ray direction (away from surface)

$\hat{d}_i$ is the incident ray direction (away from surface)

$\hat{x}$ is a unit vector in the surface plane

$\hat{y}$ is a unit vector in the surface plane perpendicular to $\hat{x}$
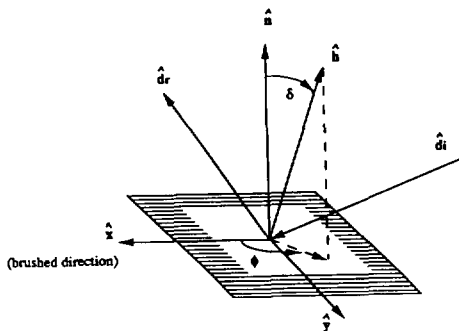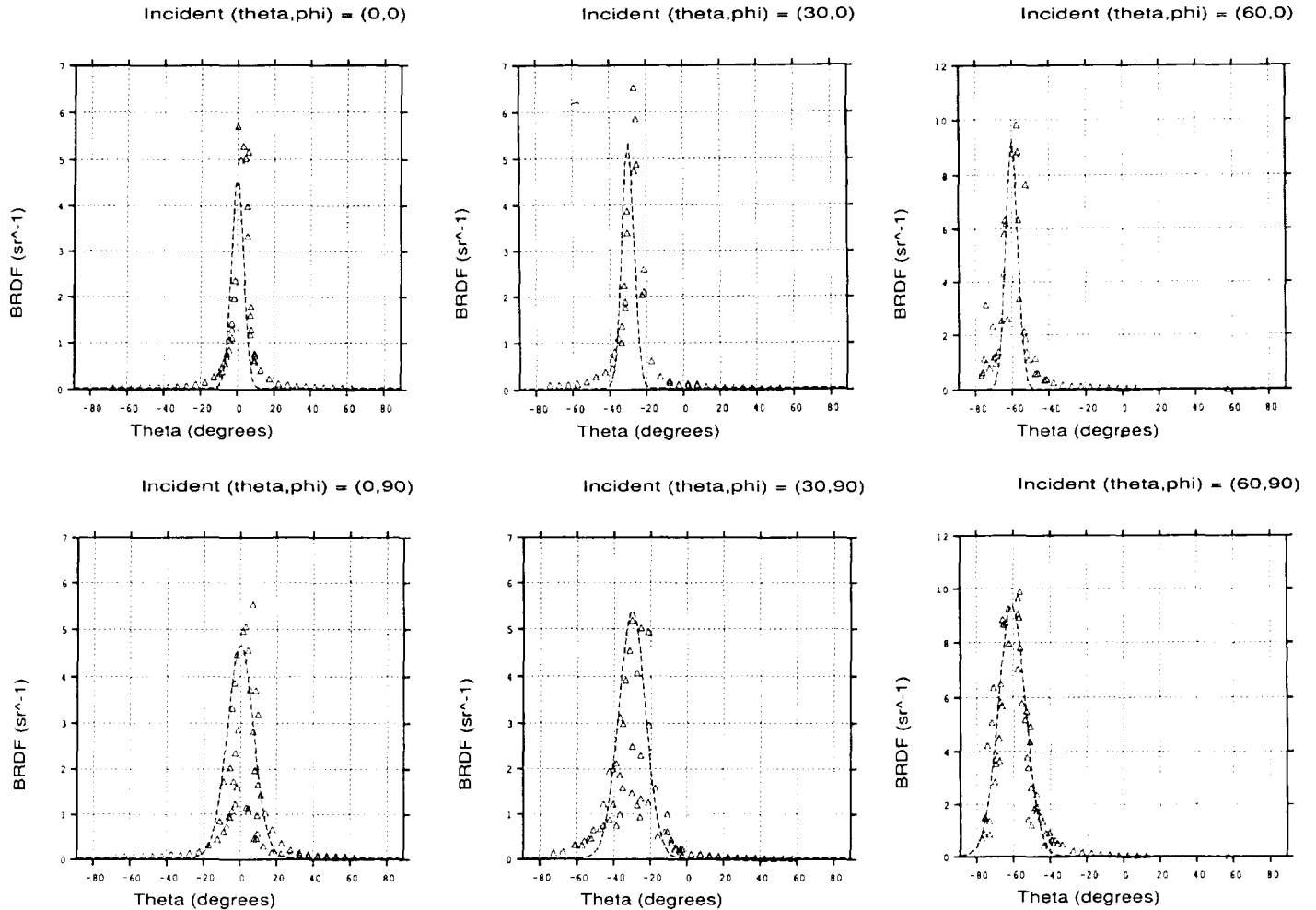

Figure 5. Angles and vectors used in reflection equations. The incident light arrives along vector $\hat{d}_i$ and is measured or simulated in direction $\hat{d}_r$. The polar angle between the half vector $\hat{h}$ and the surface normal $\hat{n}$ is δ. The azimuthal angle of $\hat{h}$ from the direction $\hat{x}$ is ϕ.

Incident (theta,phi) = (0,0)   Incident (theta,phi) = (30,0)   Incident (theta,phi) = (60,0)

Incident (theta,phi) = (0,90)   Incident (theta,phi) = (30,90)   Incident (theta,phi) = (60,90)

(BRDF (sr^-1) vs Theta (degrees))

Figure 6. Measured data and elliptical Gaussian fit for unfinished aluminum. Unfinished aluminum exhibits anisotropy from rolling during its manufacture.

As in the isotropic case, the normalization of the above anisotropic model is such that the total surface reflectance will equal the diffuse reflectance coefficient, ρ_d, plus the "rough specular" or "directional-diffuse" coefficient, ρ_s. The two other model parameters, α_x and α_y, represent the standard deviation of the surface slope in each of two perpendicular directions. Thus, all four of the model's parameters have physical meaning and can be set independently of measured data to produce a valid reflectance function. As long as the total reflectance, $\rho_d + \rho_s$, is less than 1 and the two α's are not too large, Equation 5 will yield a physically valid reflectance function.

The elliptical nature of our model arises from the two perpendicular slope distributions, and is apparent in the exponent of Equation 5a. A similar elliptical reflectance model was developed by Ohira and described by Yokoi and Toriwaki [Yokoi88], but this model was derived from that of Phong and likewise lacks physical meaning. By starting with a valid, normalized function, it is much easier to fit the model parameters to physical measurements as well as other specifications such as appearance.

Our simple four parameter model fits well the data we have gathered from anisotropic surfaces such as varnished wood and unfinished (rolled) or brushed metals. Because of its simplicity, it is easy to apply a least squares error minimization method to fit a set of parameters to measured data automatically. Automatic data fitting is essential to the economic modeling of surface reflectance for any significant database of materials. Figure 6 shows an example fit to the BRDF of an unfinished aluminum sample. Although the full hemisphere of reflected data was measured at 21 incident angles, it is difficult to visualize the 21 corresponding 3-dimensional point plots. We therefore present here only a slice of the data in the incident plane at 6 angles. The results section (6) lists the fitted parameters for this material as well as some other example surfaces.

5. Rendering Anisotropic Surfaces

The challenge to applying a new reflectance model to computer graphics is to approximate the luminance equation (1) in a manner that is unbiased and has low variance [Kajiya86]. Unfortunately, unbiased techniques (ie. pure Monte Carlo) tend to have high variance, while low variance approaches (ie. closed-form approximations) tend to be biased. To satisfy these conflicting requirements, we use a hybrid deterministic and stochastic ray tracing technique [Cook84][Cook86]. A strictly deterministic calculation of the highlight contribution of sources, similar to the widely used Whitted approximation [Whitted80], fails to pick up indirect semispecular contributions as demonstrated in Figure 7a. (Note that the crescent shape of the highlight is due to longitudinal anisotropy and not the light source.) Conversely, relying solely on stochastic sampling causes the highlights from sources to show high variance in the form of excessive noise, even with 16 samples per pixel (Figure 7b). By combining the two techniques, using a deterministic solution for source contributions and a stochastic sampling for indirect contributions, we get a clean result without compromising accuracy. Figure 7c was calculated using the hybrid technique and the same number of samples as Figure 7b. Both figures took approximately the same time to compute. (Figure 7a took less time since no sampling was required.)

The hybrid approach described reduces to the following equation:

$$L(\theta_r, \phi_r) = I \frac{\rho_d}{\pi} + L_s \rho_s + \sum_{i=1}^{N} L_i \omega_i \cos\theta_i \rho_{bd}(\theta_i, \phi_i; \theta_r, \phi_r) \qquad (6)$$

where:

I is the indirect irradiance at this point (a constant ambient level or the result of a diffuse interreflection or radiosity calculation)

L_s is the radiance value in the Monte Carlo sample direction given in Equation 7 below

L_i is the radiance of light source i

ω_i is the solid angle (in steradians) of light source i

N is the number of light sources

ρ_{bd} is the elliptical Gaussian function defined in Equation 5

In applying this technique, it is very important not to bias the sample by overcounting the specular component. Bias is easily avoided by associating a flag with the stochastically sampled specular ray. If the ray hits a light source whose contribution is being included in a closed form calculation, then the ray is not counted. Few rays are wasted in this way, since light sources occupy a small amount of the visual space in most scenes.

5.1. Stochastic Sampling of Elliptical Gaussian

Because of its simplicity, the elliptical Gaussian model adapts easily to stochastic sampling techniques. Using standard Monte Carlo integral conversion methods [Rubenstein81], we can write the following formulas for obtaining uniformly weighted sample directions for each L_s ray in Equation 6:

$$\delta = \left[\frac{-\log(u_1)}{\cos^2\phi/\alpha_x^2 + \sin^2\phi/\alpha_y^2} \right]^{1/2} \qquad (7a)$$

$$\phi = \tan^{-1}\left[\frac{\alpha_y}{\alpha_x} \tan(2\pi u_2) \right] \qquad (7b)$$

where:

δ, ϕ are the angles shown in Figure 5

u_1, u_2 are uniform random variables in the range (0,1]

notes:

The tangent and arctangent in the Equation 7a should be computed carefully so as to keep the angle in its starting quadrant.

Uniformly weighted sample rays sent according to the above distribution will correctly reproduce the specified highlight. This is much more efficient than either distributing the samples evenly and then weighting the result, or using other techniques, such as rejection sampling, to arrive at the correct scattering. Readers familiar with Monte Carlo sampling techniques will immediately appreciate the advantage of having a formula for the sample point locations -- something that is impossible with more complicated reflectance models such as He-Torrance.

6. Results

Figure 8a shows a photograph of a child's varnished wood chair with a small desk lamp immediately behind and above it. This arrangement results in a large anisotropic highlight in the seat of the chair. Figure 8b shows the closest simulation possible using a deterministic isotropic reflectance model. Figure 8c shows a hybrid simulation with the elliptical Gaussian model. Notice how the hybrid rendering technique reproduces not only the highlight from the light source, but also the semispecular reflection from the back wall in the seat of the chair.

Figure 9 shows a table with anisotropic reflections in the wood varnish and the two candle holders. The lid of the silver box shown is also anisotropic, and demonstrates the use of local control to affect the reflectance properties of an anisotropic surface. A wave function determines the orientation of the brushed direction in the box lid, producing characteristic highlights. There are four low level light sources in the scene, the two candles on the table, an overhead light source above and to the right, and the moon shining in through a window.
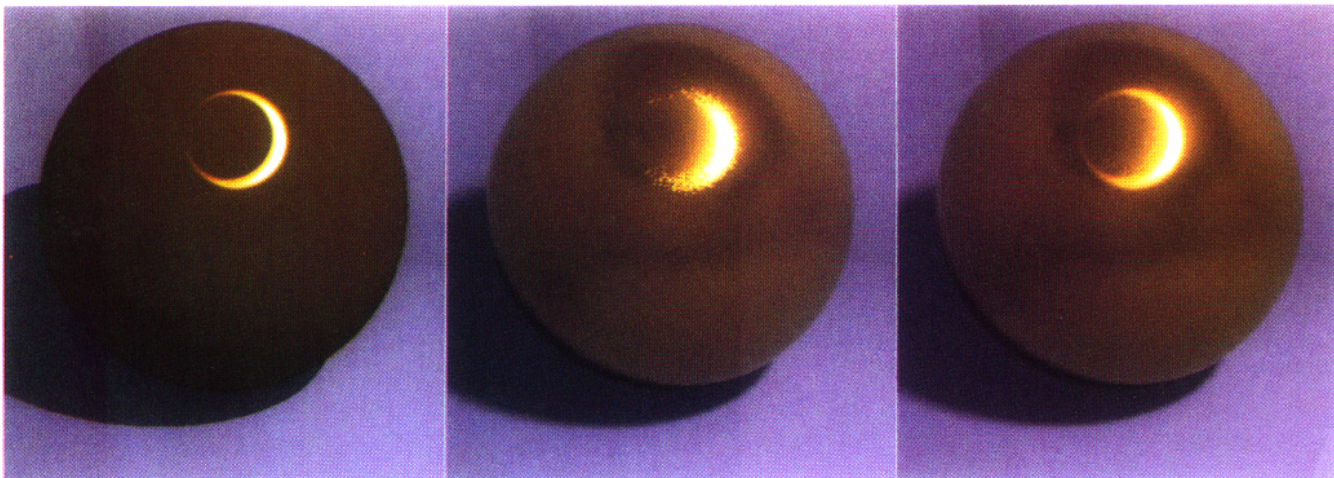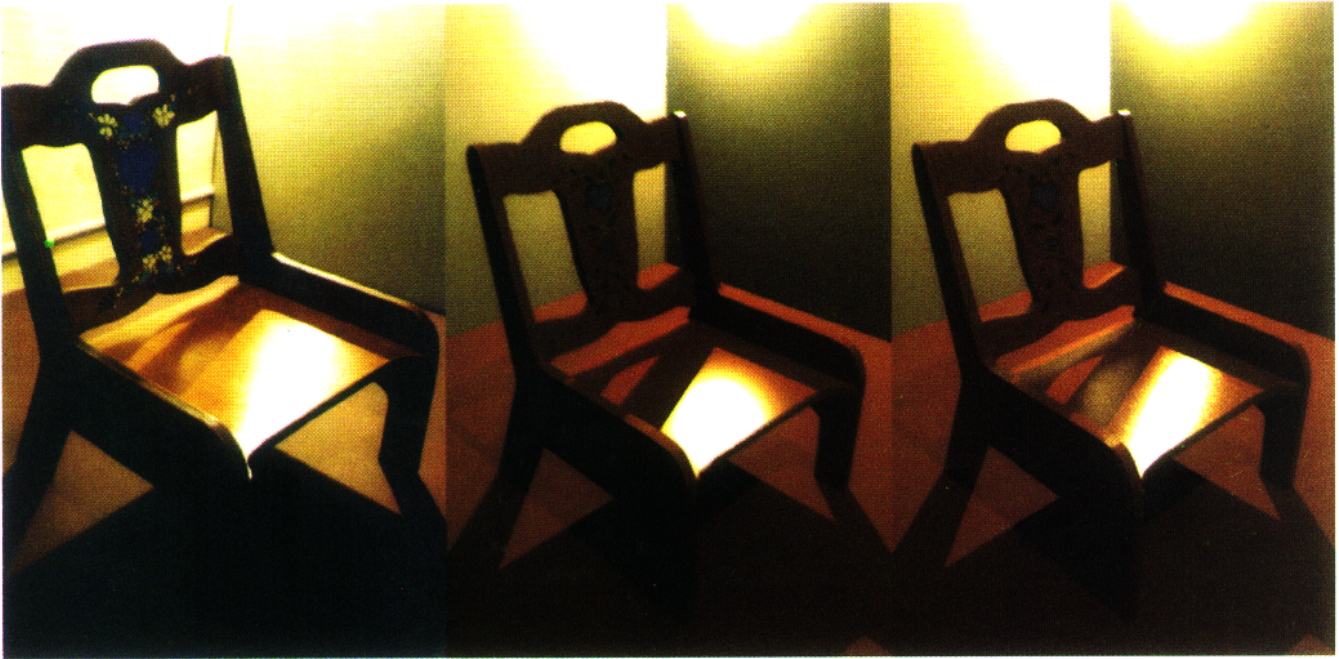

Figure 7a, 7b, 7c. Alternative rendering techniques for anisotropic reflection. 7a on the left shows deterministic technique with no sampling. 7b center shows strict Monte Carlo sampling approach. 7c on the right shows hybrid deterministic and stochastic method.

Figure 8a, 8b, 8c. Varnished wood comparison. 8a on the left shows a photograph of a child's chair. 8b center shows a simulation of the chair using the isotropic Gaussian model given in Section 4.1 with a strictly deterministic calculation. (This is similar to the appearance one might obtain using a normalized Phong reflectance model.) 8c on the right shows a hybrid deterministic and stochastic simulation of the chair using the elliptical Gaussian model from Section 4.2.

Figure 9. A table scene with anisotropic reflection in metallic and varnished wood surfaces.

The following table gives a short list of surfaces and their elliptical Gaussian fits. Color was not measured for any of the surfaces. The materials in the second half of the table are isotropic, so the two α values are the same, and Equation (4) can be used.

Material	ρ_d	ρ_s	α_x	α_y
rolled brass	.10	.33	.050	.16
rolled aluminum	.1	.21	.04	.09
lightly brushed aluminum	.15	.19	.088	.13
varnished plywood	.33	.025	.04	.11
enamel finished metal	.25	.047	.080	.096
painted cardboard box	.19	.043	.076	.085
white ceramic tile	.70	.050	.071	.071
glossy grey paper	.29	.083	.082	.082
ivory computer plastic	.45	.043	.13	.13
plastic laminate	.67	.070	.092	.092

We have also measured the reflectance functions of various painted surfaces. We found the "flat" Latex paint we tested to be very nearly diffuse, at least for incident angles up to 60°. Therefore, we present only the results from our measurements of "semi-gloss" and "gloss" Latex. Our ρ_d was around 0.45 for both the semi-gloss and the gloss paints. The value for ρ_s of the semi-gloss Latex was around 0.048 for all surfaces, and the gloss Latex had a slightly higher average of 0.059. Although ρ_d changes dramatically with the color of paint, the value for ρ_s remains fairly constant since it is determined by the index of refraction of the paint base. The values for α_x and α_y are also unaffected by paint color, but since they depend on the exact microstructure of the painted surface, they vary with the application method and the underlying material, as shown in the following two tables.

(α_x, α_y) for Latex Semi-Gloss, $\rho_s \approx 0.048$			
	brushed	rolled	sprayed
metal	(.037, .064)	(.045, .068)	(.041, .055)
sheetrock	(.078, .12)	(.083, .12)	(.096, .11)
wood	(.097, .24)	(.12, .26)	(.099, .26)

(α_x, α_y) for Latex Gloss, $\rho_s \approx 0.059$			
	brushed	rolled	sprayed
metal	(.037, .063)	(.054, .080)	(.038, .054)
sheetrock	(.10, .10)	(.12, .12)	(.10, .10)
wood	(.13, .22)	(.13, .20)	(.12, .17)

7. Conclusion

We have presented an economical new device for measuring BRDFs, and a simple reflectance model that fits a large class of materials. The imaging gonioreflectometer presented here is a working prototype, but improvements are necessary for the measurement of grazing angles and smoother materials. Likewise, the elliptical Gaussian model presented is fast and accurate for many surfaces, but there are still many materials that do not fit our function. In conclusion, although the initial efforts are promising, we hope that this work will stimulate further investigation of empirical shading models. After all, good science requires both theory and data -- one is of little use without the other.

8. Acknowledgements

9. References

[Beckmann63]
Beckmann, Petr, Andre Spizzichino, *The Scattering of Electromagnetic Waves from Rough Surfaces*, Pergamon Press, NY, 1963.

[Blinn77]
Blinn, James F., "Models of Light Reflection for Computer Synthesized Pictures," *Computer Graphics*, Vol. 11, No. 2, July 1977.

[Cabral87]
Cabral, Brian, Nelson Max, Rebecca Springmeyer, "Bidirectional Reflection from Surface Bump Maps," *Computer Graphics*, Vol. 21, No. 4, July 1987.

[Cook82]
Cook, Robert L., Kenneth E. Torrance, "A Reflectance Model for Computer Graphics," *Computer Graphics*, Vol. 15, No. 3, August 1981.

[Cook84]
Cook, Robert L., Thomas Porter, Loren Carpenter, "Distributed Ray Tracing," *Computer Graphics*, Vol. 18, No. 3, July 1984.

[Cook86]
Cook, Robert L., "Stochastic Sampling in Computer Graphics," *ACM Transactions on Graphics*, Vol. 5, No. 1, January 1986.

[He91]
He, X., K.E. Torrance, F.X. Sillion, D.P. Greenberg, "A Comprehensive Physical Model for Light Reflection," *Computer Graphics*, Vol. 25, No. 4, July 1991.

[Kajiya85]
Kajiya, James T., "Anisotropic Reflection Models," *Computer Graphics*, Vol. 19, No. 3, July 1985.

[Kajiya86]
Kajiya, James T., "The Rendering Equation," *Computer Graphics*, Vol. 20, No. 4, August 1986.

[Murray-Coleman90]
Murray-Coleman, J.F., A.M. Smith, "The Automated Measurement of BRDFs and their Application to Luminaire Modeling," *Journal of the Illuminating Engineering Society*, Winter 1990.

[Nicodemus77]
Nicodemus, F.E., J.C. Richmond, J.J. Hsia, *Geometrical Considerations and Nomenclature for Reflectance*, U.S. Department of Commerce, National Bureau of Standards, October 1977.

[Phong75]
Phong, B., "Illumination for Computer Generated Pictures," *Communications of the ACM*, Vol. 18, No. 6, June 1975.

[Poulin90]
Poulin, Pierre, Alain Fournier, "A Model for Anisotropic Reflection," *Computer Graphics*, Vol. 24, No. 4, August 1990.

[Rubenstein81]
Rubenstein, R.Y., *Simulation and the Monte Carlo Method*, J. Wiley, New York, 1981.

[Sandford85]
Sandford, Brian P., David C. Robertson, "Infrared Reflectance Properties of Aircraft Paints," *Proceedings IRIS Targets, Backgrounds, and Discrimination*, 1985.

[Sillion91]
Sillion, Francois, James Arvo, Donald Greenberg, "A Global Illumination Solution for General Reflectance Distributions," *Computer Graphics*, Vol. 25, No. 4, July 1991.

[Torrance67]
Torrance, K.E., E.M. Sparrow, "Theory for Off-Specular Reflection from Roughened Surfaces," *Journal of the Optical Society of America*, Vol. 57, No. 9, September 1967.

[Whitted80]
Whitted, Turner, "An Improved Illumination Model for Shaded Display," *Communications of the ACM*, Vol. 23, No. 6, June 1980, pp. 343-349.

[Yokoi88]
Yokoi, Shigeki, Jun-ichiro Toriwaki, "Realistic Expression of Solids with Feeling of Materials," *JARECT*, Vol. 18, 1988.